

## Static and dynamic properties of stacked Josephson junctions: Analytic solution

V. M. Krasnov

*Department of Physics, Chalmers University of Technology, S-41296, Göteborg, Sweden  
and Institute of Solid State Physics, Russian Academy of Sciences, 142432 Chernogolovka, Russia*

D. Winkler

*Department of Physics, Chalmers University of Technology, S-41296, Göteborg, Sweden*

(Received 17 April 1997)

Static and dynamic properties of stacked Josephson junctions are studied theoretically. An approximate analytic solution for a stack with arbitrary junction parameters was obtained. The analytic solution is in good agreement with numerical simulations. Characteristic penetration depths, Swihart velocities, the lower critical field, the first integral, and the free energy for a stack of nonidentical junctions were derived and studied for different parameters of the stack. We show that attractive interaction of fluxons in adjacent junctions exists in the dynamic state of the stack, leading to appearance of the “*in-phase*” state with fluxons on top of each other. In a given external magnetic field the Gibbs free energy has a number of local minima corresponding to particular fluxon distributions (modes) in the stack each representing a quasiequilibrium state. For a stack of  $N$  junctions each mode would result in  $N$  distinct flux-flow branches in the current-voltage characteristic. Taking into account that different modes with equal total number of fluxons are not identical we conclude that the total possible number of flux-flow branches can be much larger than the number of junctions in the stack. [S0163-1829(97)02337-0]

### I. INTRODUCTION

Stacked Josephson junctions (SJJ's) have attracted much attention in the last years because they are promising objects for application in cryoelectronics and they exhibit a lot of interesting physical phenomena. A particular interest in SJJ's was stimulated by the discovery of the intrinsic Josephson effect in high- $T_c$  superconductors (HTSC's) and organic superconductors.<sup>1,2</sup> The intrinsic Josephson effect in those compounds is attributed to Josephson coupling between atomic scale superconducting layers; e.g., in  $\text{Bi}_2\text{Sr}_2\text{CaCu}_2\text{O}_8$  the Josephson coupling is believed to exist between the copper-oxide double planes through the barrier formed by the Bi-O and Sr-O layers. Indeed, the intrinsic Josephson effect in HTSC's exhibit many similarities with the behavior of Josephson coupled low- $T_c$  superconducting (LTSC's) structures.

For Josephson coupled LTSC's layered structures transverse transport and magnetic properties are well studied for stacked Nb/ $\text{AlO}_x$ /Nb superconductor-insulator-superconductor (SIS) tunnel junctions<sup>3-5</sup> and for Nb/Cu proximity coupled superconductor-normal-metal-superconductor (SNS) multilayers.<sup>6-8</sup> In Nb/Cu multilayers (like in the case of HTSC's intrinsic SJJ's) the layer thickness is much less than the London penetration depth while in Nb/ $\text{AlO}_x$ /Nb SJJ's the superconducting layer thickness is typically of the order of the London penetration depth. Independent of the nature of the coupling between layers, the behavior of both Nb/ $\text{AlO}_x$ /Nb SJJ's and Nb/Cu multilayers are characterized by a pronounced phase locking phenomenon due to mutual coupling of SJJ's. For example, in Nb/Cu multilayers phase locking of ten SJJ's was achieved by applying a small external RF power.<sup>7</sup>

Among the experimental evidence for the Josephson-type

coupling between atomic layers in HTSC's we mention (i) observation of multiple “quasiparticle” branches in the  $c$ -axis current-voltage ( $I$ - $V$ ) characteristics.<sup>1,2</sup> Here, each branch is assumed to be caused by switching of an additional SJJ from the zero voltage state to the quasiparticle branch with its characteristic superconducting gap voltage. Such behavior is typical for SIS Josephson junctions connected in series<sup>9</sup> and was observed for Nb/ $\text{AlO}_x$ /Nb SJJ's.<sup>3,4</sup> The total number of quasiparticle branches in the  $I$ - $V$  curve in this case is equal to the number of junctions in the stack. (ii) Observation of Fraunhofer oscillations of the  $c$ -axis critical current<sup>1,10,11</sup> with the periodicity in magnetic field defined by the space periodicity of superconducting layers. Clear Fraunhofer oscillations of this type have been observed in Nb/Cu multilayers.<sup>8</sup> (iii) Observation of flux-flow-type  $I$ - $V$  curves in magnetic field parallel to the  $ab$  plane.<sup>12</sup> Very rich flux-flow phenomena with phase locking and multiple  $I$ - $V$  curve branches have been observed for LTSC's Nb/ $\text{AlO}_x$ /Nb SJJ's (Ref. 4) and Nb/Cu multilayers.<sup>8</sup> For Nb/Cu multilayers the number of observed flux-flow branches in the  $I$ - $V$  characteristic exceeds the number of junctions in the multilayer.<sup>8</sup> (iv) observation of Josephson plasma wave resonances in HTSC's.<sup>13</sup>

Theoretically, properties of layered superconductors with Josephson coupling between layers were studied in a number of papers, see, e.g., Refs. 14–21. Among the recent developments in this direction we mention realization of collective plasma excitations<sup>20</sup> and charging effects<sup>21</sup> in HTSC's SJJ's.

In the current paper we study theoretically the static and dynamic properties of SJJ's using the formalism of Sakai, Bodin, and Pedersen.<sup>18</sup> A simple approximate analytic solution for a stack with arbitrary parameters was obtained. The analytic solution is in good agreement with numerical simulations. Characteristic penetration depths and Swihart veloci-

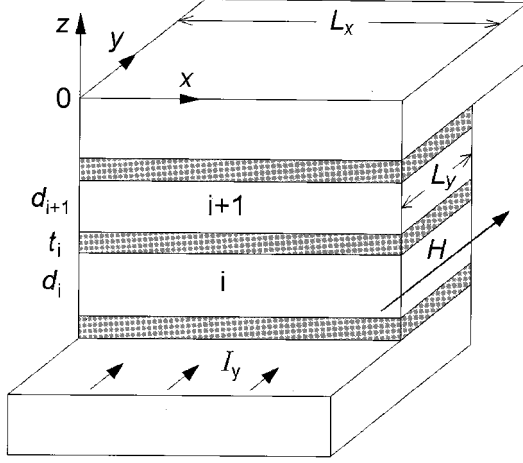


FIG. 1. Schematic drawing of the stacked Josephson junctions.

ties, the lower critical field, the first integral, and the free energy were derived and studied for different parameters of the stack.

From our analysis we show the existence of *attractive fluxon interaction* in the adjacent junctions in the dynamic state of the SJJ so that the “in-phase” state<sup>18</sup> with fluxons on top of each other become possible at high enough fluxon velocity. We show that in a given external magnetic field there is a number of quasiequilibrium fluxon states (modes) corresponding to a particular fluxon distribution in SJJ’s. For a stack of  $N$  junctions each mode would result in  $N$  distinct flux-flow branches in the  $I$ - $V$  characteristic. Taking into account that different modes with equal total number of fluxons are not identical we conclude that the total possible number of flux-flow branches can be much larger than the number of junctions in the stack.

## II. GENERAL RELATIONS

We consider a stack of  $N$  Josephson junctions (JJ’s) with the tunnel barrier parallel to the  $x$ - $y$  plane and the  $z$ -axis directed perpendicular to the barrier. An external magnetic field,  $H$ , is applied parallel to the junction plane in the  $y$ -axis direction.  $L_x$  and  $L_y$  are the junction lengths along the  $x$  and  $y$  axes, respectively. A sketch of the stack is shown in Fig. 1. We will assume that  $L_y$  is smaller than the Josephson penetration depth,  $\lambda_J$ . We number the junctions in the stack incremental in the  $z$ -axis direction so that the bottom junction has the number  $i=1$  and the top junction corresponds to  $i=N$ . Superconducting layers composing the JJ’s are also numbered in the  $z$ -axis direction so that the bottom layer has the number  $i=1$  and the top layer has the number  $i=N+1$ . Thus the JJ number  $i$  is composed by the layers number  $i$  and  $i+1$ , see Fig. 1. The superconducting layers are characterized by the London penetration depth  $\lambda_{si}$  and the thickness  $d_i$  and junctions are characterized by the tunnel barrier thickness  $t_i$  and the critical current density  $J_{ci}$ . Hereafter, the subscript  $i$  on the quantity represent its number.

Integration of the vector potential over the contour covering the tunnel barrier provides a relationship between the gauge-invariant phase difference  $\varphi_i$  and the local magnetic inductance  $B_i$  inside the junction.<sup>18</sup>

$$\frac{\Phi_0}{2\pi} \frac{\partial}{\partial x} \varphi = \mathbf{A}_1 \cdot \mathbf{B}_y, \quad (1a)$$

$$\frac{\Phi_0}{2\pi} \frac{\partial}{\partial y} \varphi = -\mathbf{A}_1 \cdot \mathbf{B}_x, \quad (1b)$$

where  $\Phi_0$  is the flux quantum and

$$\varphi = \begin{pmatrix} \varphi_1 \\ \varphi_2 \\ \vdots \\ \varphi_i \\ \vdots \\ \varphi_{N-1} \\ \varphi_N \end{pmatrix}, \quad \mathbf{B} = \begin{pmatrix} H \\ B_1 \\ B_2 \\ \vdots \\ B_i \\ \vdots \\ B_{N-1} \\ B_N \\ H \end{pmatrix},$$

$$\mathbf{A}_1 = \begin{pmatrix} -S_1 & \vdots \\ 0 & \mathbf{A} & 0 \\ \vdots & & -S_{N+1} \end{pmatrix}, \quad (2)$$

$$\mathbf{A} = \begin{pmatrix} \Lambda_1 & -S_2 & 0 & \cdots & & 0 \\ -S_2 & \Lambda_2 & -S_3 & 0 & \cdots & \\ 0 & \ddots & \ddots & \ddots & 0 & \cdots \\ \cdots & 0 & -S_i & \Lambda_i & -S_{i+1} & 0 & \cdots \\ \cdots & 0 & \ddots & \ddots & \ddots & \ddots & 0 \\ & \cdots & 0 & -S_{N-1} & \Lambda_{N-1} & -S_N \\ 0 & \cdots & 0 & 0 & -S_N & \Lambda_N \end{pmatrix}, \quad (3)$$

and

$$\Lambda_i = t_i + \lambda_{si} \coth(d_i/\lambda_{si}) + \lambda_{s_{i+1}} \coth(d_{i+1}/\lambda_{s_{i+1}}), \quad (4)$$

$$S_i = \lambda_{si} \operatorname{cosech}(d_i/\lambda_{si}). \quad (5)$$

The inner part of the matrix  $\mathbf{A}_1$ , Eq. (2), is identical to the matrix  $\mathbf{A}$ , Eq. (3).

Differentiating Eqs. (1a) and (1b) with respect to the  $x$  and  $y$  coordinate we obtain the coupled “sine-Gordon” equation describing the behavior of stacked JJ’s:<sup>18</sup>

$$\frac{\Phi_0 c}{8\pi^2} \left( \frac{\partial^2}{\partial x^2} + \frac{\partial^2}{\partial y^2} \right) \varphi = \mathbf{A} \cdot \mathbf{J}_z, \quad (6)$$

where

$$\mathbf{J}_z = \begin{pmatrix} J_{z1} \\ J_{z2} \\ \vdots \\ J_{zi} \\ \vdots \\ J_{zN-1} \\ J_{zN} \end{pmatrix},$$

$$J_{zi} = J_{ci} \sin(\varphi_i) + \frac{\Phi_0 C_i}{2\pi c} \frac{\partial^2 \varphi_i}{\partial t^2} + \frac{\Phi_0}{2\pi c R_i} \frac{\partial \varphi_i}{\partial t}. \quad (7)$$

Here  $J_{zi}$  is the Josephson current in junction  $i$ ,  $C_i$  and  $R_i$  are the junction capacitance and the quasiparticle resistance, respectively, per unit area of the junction.

Equation (6) can be simplified for the case of small  $L_y$ . We restrict ourselves to consider the ‘‘overlap’’ geometry for the stack. Let  $J_{yi}$  be the bias current uniformly injected in the layer  $i$  along the  $y$  axis, see Fig. 1. Using the Biot-Savart law we can write for the  $x$  component of the magnetic induction

$$B_{xi} = \frac{2\pi}{c} \left[ \sum_1^i I_{yj} - \sum_{i+1}^{N+1} I_{yj} \right], \quad (8)$$

where  $I_{yj} = \int J_{yj} dz_j$ . Having substituted Eq. (8) into Eq. (1b) and differentiating with respect to  $y$  we obtain

$$\begin{aligned} \frac{\Phi_0 c}{4\pi^2} \frac{\partial^2}{\partial y^2} \varphi_i = \frac{1}{2L_y} & \left[ (\Lambda_i - S_i - S_{i+1}) \left( \sum_{i+2}^{N+1} \Delta I_{yj} - \sum_1^{i-1} \Delta I_{yj} \right) \right. \\ & + (\Lambda_i - S_i + S_{i+1}) \Delta I_{yi+1} - (\Lambda_i + S_i \\ & \left. - S_{i+1}) \Delta I_{yi} \right]. \quad (9) \end{aligned}$$

In deriving this equation we have substituted the derivative of  $I_{yi}$  by the finite difference  $\partial I_{yi} / \partial y \approx \Delta I_{yi} / L_y$ , where  $\Delta I_{yi} = I_{yi}(L_y) - I_{yi}(0)$ . Equation (9) makes it possible to take into account different biasing configurations, e.g., biasing via middle electrodes. In the usual case when the stack is biased via the top and the bottom layers the set of Eqs. (9) is reduced to that of Ref. 18.

Subtraction of Eq. (9) from Eq. (6) yields the final one-dimensional coupled sine-Gordon equation for the phase distribution in the stack. Equation (6) should be supplemented by the boundary conditions at  $x=0$ , and  $x=L_x$  which are given by Eq. (1a) with  $B_{yi} \equiv H$ .

As we will show below the solution of the coupled sine-Gordon equations for SJJ's allows different quasiequilibrium states (which we will refer to as ‘‘modes’’) characterized by the different number of fluxons in the junctions. For the stack of  $N$  junctions we will use a string  $(n_1, \dots, n_i, \dots, n_N)$  as a short notation of those modes, where  $n_i$  is a number of fluxons in the junction  $i$ . For example, mode (1,0) represent the state with a single fluxon in junction 1 for a double SJJ.

### A. The first integral

In the static case Eq. (6) has a first integral which can be written in a compact form

$$\frac{\Phi_0 c}{16\pi^2} \varphi' * \mathbf{A}^{-1} \varphi' + \sum J_{ci} \cos(\varphi_i) = \mathbf{C}, \quad (10)$$

where  $\mathbf{C}$  is a constant. Here the symbol ‘‘prime’’ on the quantity denotes its spatial derivative and the symbol \* denotes the transposition so that  $\varphi' *$  is a string of  $\varphi'_i$ . For double SJJ's the first integral is equal to

$$\begin{aligned} \frac{\lambda_{J1}^2 J_{c1}}{(1-S^2)} \left[ \frac{(\varphi_1')^2}{2} + \frac{\Lambda_1}{\Lambda_2} \frac{(\varphi_2')^2}{2} + \frac{S_2}{\Lambda_2} \varphi_1' \varphi_2' \right] \\ + J_{c1} \cos(\varphi_1) + J_{c2} \cos(\varphi_2) = \mathbf{C}, \quad (11) \end{aligned}$$

which for identical junctions reduces to that of Ref. 22.

### B. Approximate analytic solution

In general the solution of Eq. (6) is quite complicated. However, it is possible to construct an approximate solution providing a fairly good approximation in the whole space-time region. We will show the procedure for obtaining the approximate solution for the example of double stacked JJ's. The extension for the case of an arbitrary number of stacked JJ's is straightforward.

For low viscosity the system of equations for double SJJ's is

$$\begin{aligned} \lambda_{J1}^2 \frac{\partial^2 \varphi_1}{\partial x^2} - \frac{1}{\omega_{p1}^2} \frac{\partial^2 \varphi_1}{\partial t^2} + \frac{C_2 S_2}{C_1 \Lambda_1 \omega_{p1}^2} \frac{\partial^2 \varphi_2}{\partial t^2} \\ = \sin(\varphi_1) - \frac{J_{c2} S_2}{J_{c1} \Lambda_1} \sin(\varphi_2), \\ \lambda_{J1}^2 \frac{\partial^2 \varphi_2}{\partial x^2} - \frac{C_2 \Lambda_2}{C_1 \Lambda_1} \frac{1}{\omega_{p1}^2} \frac{\partial^2 \varphi_2}{\partial t^2} + \frac{S_2}{\Lambda_1 \omega_{p1}^2} \frac{\partial^2 \varphi_1}{\partial t^2} \\ = \frac{J_{c2} \Lambda_2}{J_{c1} \Lambda_1} \sin(\varphi_2) - \frac{S_2}{\Lambda_1} \sin(\varphi_1). \quad (12) \end{aligned}$$

Here  $\lambda_{J1}$  and  $\omega_{p1}$  are the Josephson penetration depth and the plasma frequency, respectively, of the single junction 1,  $\lambda_{J1}^2 = \Phi_0 c / 8\pi^2 J_{c1} \Lambda_1$ ,  $\omega_{p1}^2 = (\Phi_0 / 2\pi c) (C_1 / J_{c1})$ .

The coupling strength can be described by a dimensionless coupling parameter

$$S^2 = \frac{S_2^2}{\Lambda_1 \Lambda_2}. \quad (13)$$

First we consider a special single fluxon solution in the form

$$\sin(\varphi_1) = \kappa \sin(\varphi_2), \quad (14)$$

which allows the  $2\pi$  total phase shift in one JJ and zero total phase shift in the other JJ. Here  $\kappa$  is a constant parameter which should be determined from Eq. (12). For definition we assume that the fluxon is situated in junction 1. In this case  $\varphi_2$  is small for the arbitrary coupling parameter  $S$  and the left-hand side of Eq. (12) can be linearized with respect to  $\varphi_2$ ,

$$\varphi_1'' \approx \kappa \varphi_2''.$$

After this, Eqs. (12) are reduced to an ordinary sine-Gordon equation

$$F''_{\xi\xi} = \sin(F(\xi)), \quad (15)$$

which has a well-known fluxon solution in the form of a traveling soliton

$$F = 4 \arctan(\exp(\xi)), \quad \xi = \frac{x - ut}{\lambda_J \gamma}. \quad (16)$$

Here  $u$  is the velocity of the soliton and  $\gamma$  is the Lorentz factor,  $\gamma^2 = 1 - (u/\tilde{c})^2$ ,  $\tilde{c} = \lambda_J \omega_p$  is the Swihart velocity.

Substituting Eq. (14) into Eq. (12) we obtain that the parameter  $\kappa$  in Eq. (14) is a solution of the quadratic equation:

$$\frac{S_2}{\Lambda_1} \kappa^2 + \kappa \left[ 1 - \frac{J_{c2}\Lambda_2}{J_{c1}\Lambda_1} + \frac{u^2}{\tilde{c}_{01}^2} \frac{\Lambda_2}{\Lambda_1} \left( \frac{J_{c2}}{J_{c1}} - \frac{C_2}{C_1} \right) (1 - S^2) \right] - \frac{J_{c2}S_2}{J_{c1}\Lambda_1} = 0, \quad (17)$$

which always has two roots,  $\kappa_1$  and  $\kappa_2$ . Here  $\tilde{c}_{01} = \lambda_{J1} \omega_{p1}$  is the Swihart velocity of the single junction 1. Thus Eq. (12) has two special single fluxon solutions

$$\varphi_1 = F_1(\lambda_1), \quad \varphi_2 = 1/\kappa_1 \arcsin(\sin(F_1)), \quad (18a)$$

$$\varphi_1 = F_2(\lambda_2), \quad \varphi_2 = 1/\kappa_2 \arcsin(\sin(F_2)), \quad (18b)$$

where  $F_{1,2}$  are given by Eq. (16) with

$$\lambda_J^2 \gamma^2 = \lambda_{1,2}^2 \left( 1 - \frac{u^2}{\tilde{c}_{1,2}^2} \right), \quad (19)$$

where the characteristic penetration depths are

$$\lambda_{1,2}^2 = \frac{\lambda_{J1}^2}{1 + \kappa_{2,1} S_2 / \Lambda_1}, \quad (20)$$

and Swihart velocities are

$$\tilde{c}_{1,2}^2 = \frac{\tilde{c}_{01}^2}{1 + \kappa_{2,1} (C_2 J_{c1} S_2) / (C_1 J_{c2} \Lambda_1)}. \quad (21)$$

For the case of identical junctions

$$\kappa_{1,2} = \mp 1, \quad \lambda_{1,2} = \lambda_J / \sqrt{1 \pm S} \quad \text{and} \quad \tilde{c}_{1,2} = \tilde{c}_{01} / \sqrt{1 \pm S},$$

which coincides with the previous result.<sup>18</sup>

The special solution Eq. (18) can only be realized in the dynamic case of high fluxon velocity  $\tilde{c}_1 < u < \tilde{c}_2$  when one of the solutions  $F_1, F_2$  becomes degenerate as will be discussed later.

In order to find the solution for lower velocities we consider the linearized Eq. (12) with  $\sin(\varphi_1) \approx \varphi_1$  and  $\sin(\varphi_2) \approx \varphi_2$ . It can be shown that the general solution of the linearized equation is given by a linear combination of  $F_1$  and  $F_2$

$$\varphi_1 = aF_1 + bF_2, \quad (22a)$$

$$\varphi_2 = cF_1 + dF_2, \quad (22b)$$

where

$$a = \kappa_1 c,$$

$$b = \kappa_2 d. \quad (23)$$

Coefficients  $a, b, c, d$  should be chosen for a particular fluxon configuration in the stack from the condition of having a particular total phase shift at  $x = \pm \infty$  (we suppose that the JJ's are long enough to avoid the problems related with the fluxon interaction with the edges of the JJ). Namely for a single fluxon in junction 1 and no fluxons in junction 2 the total phase shift  $\varphi_1(+\infty) - \varphi_1(-\infty) = 2\pi$  and  $\varphi_2(+\infty) - \varphi_2(-\infty) = 0$ , which gives two additional conditions for the coefficients of Eq. (22),

$$a + b = 1,$$

$$c + d = 0. \quad (24)$$

From Eqs. (23) and (24) we finally obtain a unique solution

$$\varphi_1 = \frac{\kappa_1 F_1 - \kappa_2 F_2}{\kappa_1 - \kappa_2}, \quad (25)$$

$$\varphi_2 = \frac{F_1 - F_2}{\kappa_1 - \kappa_2}.$$

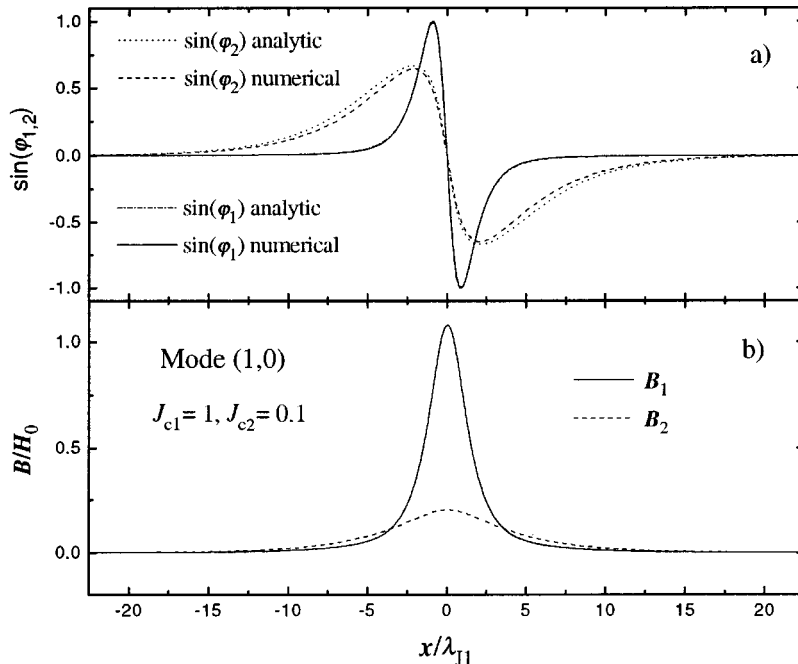


FIG. 2. Spatial distributions of (a)  $\sin(\varphi)$ , and (b) magnetic induction  $B$ , in the static case with a single fluxon in junction 1. Parameters of the stack are  $J_{c1} = 1$ ,  $J_{c2} = 0.1$ ,  $\lambda_{s1} = \lambda_{s2} = \lambda_{s3} = 0.1\lambda_{J1}$ ,  $d_1 = d_2 = d_3 = t_1 = t_2 = 0.01\lambda_{J1}$ ,  $S \approx 0.5$ . (a) Solid and dashed curves represent solutions for  $\sin(\varphi_1)$  and  $\sin(\varphi_2)$  obtained by numerical simulations. Dashed-dotted and dotted curves represent the approximate analytical solution for  $\sin(\varphi_1)$  and  $\sin(\varphi_2)$ . The agreement between the analytical and the numerical solutions for  $\varphi_1$  is so good that they can hardly be distinguished in the figure.

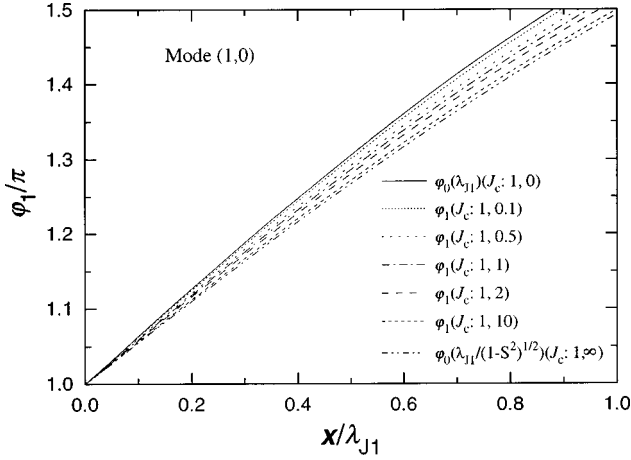


FIG. 3. Spatial distributions of  $\varphi_1$  at the origin of the fluxon for different values of  $J_{c2}$  obtained by numerical simulations. Parameters of the stack are  $J_{c2}=0,0.1,0.5,1,2,10,\infty$  from the top to the bottom curve, respectively; and  $J_{c1}=1$ ,  $\lambda_{s1}=\lambda_{s2}=\lambda_{s3}=0.1\lambda_{J1}$ ,  $d_1=d_2=d_3=t_1=t_2=0.01\lambda_{J1}$ ,  $S\approx 0.5$ . The top and bottom curves represent also the solution for a single JJ,  $\varphi_0$ , with  $\lambda_J=\lambda_{J1}$  and  $\lambda_0=\lambda_{J1}/\sqrt{1-S^2}$ .

Equation (25) provide a fairly good approximation for  $\varphi_1$  since it satisfies asymptotically Eq. (12) for  $x\ll -1$ ,  $x\sim 0$  and  $x\gg 1$  and  $\varphi_2$  satisfies asymptotically Eq. (12) for  $x\ll -1$  and  $x\gg 1$  and has a correct value,  $\varphi_2=0$ , at  $x=0$ .

Figures 2(a) and 2(b) show calculated spatial distributions of  $\sin(\varphi)$  and the magnetic induction  $B$ , respectively, in the static ( $u=0$ ) case with a single fluxon in junction 1. Parameters of the stack are  $J_{c1}=1$ ,  $J_{c2}=0.1$ ,  $\lambda_{s1}=\lambda_{s2}=\lambda_{s3}=0.1\lambda_{J1}$ ,  $d_1=d_2=d_3=t_1=t_2=0.01\lambda_{J1}$ , and  $S\approx 0.5$ . Solid and dashed curves in Fig. 2(a) represent the solution for  $\sin(\varphi_1)$  and  $\sin(\varphi_2)$ , respectively, obtained by numerical simulation of Eq. (12). Dashed-dotted and dotted curves in Fig. 2(a) represent the approximate analytical solution for  $\sin(\varphi_1)$  and  $\sin(\varphi_2)$ , respectively, obtained from Eq. (25). For  $\varphi_1$  the agreement between the approximate analytical solution and the numerical simulations is so good that they can hardly be distinguished in the figure.

An important consequence of Eq. (25) is that the phase distribution in both junctions is not described by a single length. This can clearly be seen in Fig. 2(a). At large distances from the fluxon origin the decay length is given by the largest of  $\lambda_{1,2}$  and at  $x=0$  we can identify the effective penetration depth  $\lambda_0$  equalizing the spatial derivative,  $\varphi'_1(x=0)$ , to that of a single soliton, Eq. (16)

$$\lambda_0^{-1} = \frac{\kappa_1\lambda_1^{-1} - \kappa_2\lambda_2^{-1}}{\kappa_1 - \kappa_2}. \quad (26)$$

$\lambda_0$  varies from  $\lambda_{J1}$  to  $\lambda_{J1}/\sqrt{1-S^2}$  when  $J_{c2}/J_{c1}$  varies from 0 to  $\infty$ . This is illustrated in Fig. 3 in which spatial distributions of the phase  $\varphi_1$  at the origin of the fluxon,  $x=0$ , are shown for different values of  $J_{c2}$ . The curves were obtained by numerical simulation of Eq. (12). Parameters of the stack are  $J_{c2}=0, 0.1, 0.5, 1, 2, 10, \infty$  from the top to the bottom curve, respectively. The current density is normalized to the critical current density in JJ1,  $J_{c1}=1$ , and  $\lambda_{s1}=\lambda_{s2}=\lambda_{s3}=0.1\lambda_{J1}$ ,  $d_1=d_2=d_3=t_1=t_2=0.01\lambda_{J1}$ ,  $S\approx 0.5$ .

Table I summarizes the characteristic parameters of a double stack for different values of  $J_{c2}$  and  $J_{c1}=1$  and for the coupling parameter  $S=0.5$  corresponding to the maximum coupling in the case of a thin layered stack,  $d_i\ll\lambda_{si}$ . The lengths are normalized to  $\lambda_{J1}$ , the velocities are normalized to  $\tilde{c}_{01}$ , and  $\tilde{c}_{02}$  is the Swihart velocity of a single junction 2. We note that for  $J_{c2}/J_{c1}<1$ ,  $\tilde{c}_2$  becomes purely imaginary which means that the  $F_2$  component cannot propagate and in the dynamic state the single fluxon solution is given by Eq. (18a). In general, this is a consequence of the fact that mode (1,0) for  $J_{c2}/J_{c1}<1$  is unstable since it is more favorable to have a fluxon in a weaker junction and the mode (0,1) will be realized instead.

For the case of  $N$  not identical SJJ's there are  $N$  different characteristic lengths, Eq. (20) and velocities, Eq. (21) where the parameters  $\kappa_j$ ,  $j=1,2,\dots,N$  should be obtained from Eq. (6).

### C. Free energy

The free energy of the stack is the sum of the kinetic energy of supercurrents, the magnetic energy, and the Josephson coupling energy.

The free-energy density of electrode  $i$  is given by

$$\mathbf{F}_{Si} = \frac{1}{8\pi} \int [B^2 + \lambda_{si}^2 \text{rot}^2 B] dz = \frac{\lambda_{si}}{8\pi} \left[ (B_i^2 + B_{i-1}^2) \times \coth\left(\frac{d_i}{\lambda_{si}}\right) - 2B_i B_{i-1} \text{cosech}\left(\frac{d_i}{\lambda_{si}}\right) \right]. \quad (27)$$

The free-energy density stored in the Josephson junction  $i$  is

$$\mathbf{F}_{Ji} = \frac{B_i^2 t_i}{8\pi} + \frac{\Phi_0}{2\pi c} J_{ci} [1 - \cos(\varphi_i)]. \quad (28)$$

TABLE I. Characteristic parameters of a double stack for different values of  $J_{c2}$  and  $J_{c1}=1$  and for the coupling parameter  $S=0.5$ .

$J_{c2}$	$\lambda_{J2}$	$\kappa_1$	$\kappa_2$	$\lambda_1$	$\lambda_2$	$\lambda_0$	$\tilde{c}_{02}$	$\tilde{c}_1$	$\tilde{c}_2$
0	$\infty$	-2	0	1	$\infty$	1	$\infty$	0.894	$i0$
0.1	3.162	-1.854	0.054	0.987	3.700	1.008	10	0.887	$i0.348$
0.5	1.414	-1.366	0.366	0.919	1.776	1.024	2	0.856	$i1.653$
1	1	-1	1	0.817	1.414	1.035	1	0.817	1.414
2	0.707	-0.732	2.732	0.6501	1.256	1.049	0.5	0.771	1.106
10	0.316	-0.539	18.54	0.3120	1.170	1.086	0.1	0.720	1.014
$\infty$	0	-0.5	$\infty$	0	1.155	1.155	0	0.707	1

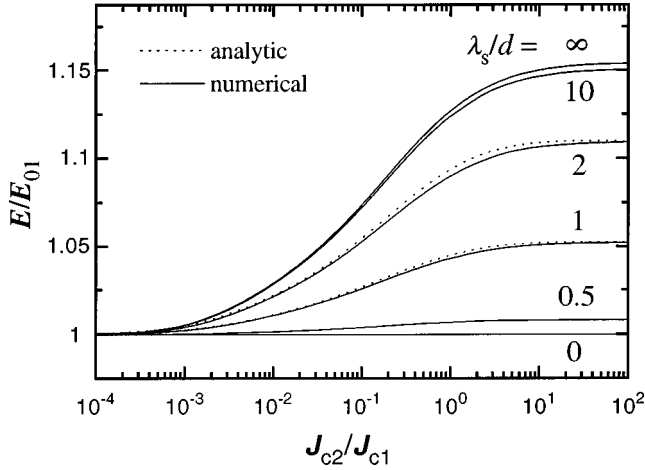


FIG. 4. The free energy of a single fluxon in junction 1, as a function of  $J_{c2}/J_{c1}$  for several layer thicknesses and coupling parameters from  $S=0$  ( $\lambda_s/d=0$ ) to  $S=0.5$  ( $\lambda_s/d=\infty$ ). Solid lines represent the result of the numerical simulation and dotted lines were obtained using the approximate analytic solution. The energy is normalized to the fluxon energy in a single JJ.

Taking a sum over the whole stack, expressing  $\mathbf{B}$  via  $\varphi'$  from Eq. (1a), and using the first integral, Eq. (10), we obtain a particularly simple expression for the free-energy density of the stack

$$\begin{aligned} \mathbf{F} &= \frac{\Phi_0}{2\pi c} \left[ \frac{\Phi_0 c}{16\pi^2} \varphi'^* \mathbf{A}^{-1} \varphi' + \sum_{i=1}^N J_{ci} [1 - \cos(\varphi_i)] \right] + E_H \\ &= \frac{\Phi_0}{2\pi c} \left[ \mathbf{C} + \sum J_{ci} [1 - 2 \cos(\varphi_i)] \right] + E_H, \end{aligned} \quad (29)$$

where  $\mathbf{C}$  is the constant in the first integral, Eq. (10) and

$$\begin{aligned} E_H &= \frac{1}{8\pi} \left\{ H^2 \left[ \lambda_{s1} \coth\left(\frac{d_1}{\lambda_{s1}}\right) + \lambda_{sN+1} \coth\left(\frac{d_{N+1}}{\lambda_{sN+1}}\right) \right] \right. \\ &\quad \left. - \mathbf{H}_S^* \mathbf{A}^{-1} \mathbf{H}_S \right\}. \end{aligned} \quad (30)$$

Here  $\mathbf{H}_S^*$  is a string  $(HS_1, 0, \dots, 0, HS_{N+1})$ ; thus  $E_H$  contains only terms  $\sim H^2$ . The total energy  $E$  is obtained by integration of Eq. (29) along the stack length ( $x$  axis). Figure 4 shows the total energy of a single fluxon in junction 1, mode (1,0), as a function of  $J_{c2}/J_{c1}$  for  $H=0$  and for several layer thicknesses and coupling parameters from  $S=0$  ( $\lambda_s/d=0$ ) to  $S=0.5$  ( $\lambda_s/d=\infty$ ). Solid lines represent the result of numerical simulation of Eq. (12) and dotted lines were obtained using the approximate analytic solution, Eq. (25). Once again a good agreement between the approximate analytical solution and the numerical simulation is seen. The energy is normalized to the fluxon energy in a single junction

$$E_0 = 8 \frac{\Phi_0 J_c \lambda_J}{2\pi c}. \quad (31)$$

Thus, from Fig. 4 it is seen that the fluxon energy in the stack is always higher than that of a single junction in qualitative agreement with Ref. 22 but in disagreement with Ref. 23. However, we cannot directly compare our results since we

have considered a single fluxon mode, while in Ref. 22 estimations were made for a special in-phase (1,1) mode and out-of-phase (1,-1) mode. The additional fluxon energy for the SJJ has two main contributions: (i) Josephson energy of junction 2 and, (ii) the change of the effective Josephson penetration depth with respect to that of the uncoupled junction. As can be seen from Table I, the latter contribution dominates for  $J_{c2} \rightarrow 0$  and  $J_{c2} \rightarrow \infty$  when the Josephson penetration depth is equal to  $\lambda_0$  and the Josephson energy of the second JJ is negligible. Since the fluxon energy is localized in the fluxon core the second contribution is defined by  $\lambda_0$ , Eq. (26) so that  $E/E_0 \sim \lambda_0/\lambda_{J1}$  and the maximum fluxon energy is equal to  $E_0/\sqrt{1-S^2}$ . This is in agreement with Fig. 4.

#### D. The lower critical field

Knowing the fluxon free energy, Eq. (29) we can derive the lower critical field,  $H_{c1}$ , of the stack, i.e., the magnetic field at which the fluxon state becomes thermodynamically stable. The thermodynamic equilibrium for a given  $H$  is achieved in the minimum of the Gibbs free energy,

$$\mathbf{G} = \mathbf{F} - \frac{BH}{4\pi}. \quad (32)$$

For bulk superconductors or JJ's with thick electrodes this equation provides a simple relationship between the fluxon free energy and the lower critical field:

$$H_{c0} = 4\pi E/\Phi_0. \quad (33)$$

However, this equation cannot directly be applied to SJJ's. The reason is that in order to achieve a coupling between the junctions, the superconducting layers should be made thin compared to the London penetration depth, see Eqs. (4), (5), and (13). Under this condition, a particular JJ in the stack contains only a fraction of the flux quantum. Thus, for determination of  $H_{c1}$  we should estimate the total flux carried by a fluxon.

First we consider a single junction. In this case the total flux of a single fluxon is equal to

$$\Phi = \Phi_0 \frac{\Lambda_1^*}{\Lambda_1}, \quad (34)$$

where

$$\Lambda_i^* = \Lambda_i - S_i - S_{i+1} \quad (35)$$

is the effective magnetic length of the junction. For the limiting cases of thick layers,  $d_i/\lambda_{si} \gg 1$ ,  $\Lambda_i^* \cong \Lambda_i$ , and as expected the fluxon carries the whole flux quantum. For thin layers,  $d_i/\lambda_{si} \ll 1$ ,  $\Lambda_i^* \cong t_i + d_i/2 + d_{i+1}/2$  and the fluxon carries only a tiny fraction of  $\Phi_0$ . The lower critical field of a single JJ is given by

$$H_{c1} = \frac{4\pi E}{\Phi}, \quad (36)$$

which regarding Eqs. (34) and (35) can be considerably larger than  $H_{c0}$ , Eq. (33). This is due to the fact that the magnetic field can freely penetrate the JJ with thin electrodes

without induction of Josephson screening currents. In turn, this is due to the reduction of the effective magnetic length  $\Lambda^*$ , see Eq. (35).

To estimate the total flux for the case of a stack we should consider the spatial distribution of  $B$  in the stack. For a double stack we can write using Eq. (1a)

$$B_1 = \frac{\Phi_0}{2\pi} \left[ \frac{\Lambda_2 \varphi'_1 + S_2 \varphi'_2}{\Lambda_1 \Lambda_2 (1-S^2)} \right] + H \left[ \frac{S_1 \Lambda_2 + S_2 S_3}{\Lambda_1 \Lambda_2 (1-S^2)} \right] = B_{f1} + A_1 H, \quad (37a)$$

$$B_2 = \frac{\Phi_0}{2\pi} \left[ \frac{S_2 \varphi'_1 + \Lambda_1 \varphi'_2}{\Lambda_1 \Lambda_2 (1-S^2)} \right] + H \left[ \frac{S_3 \Lambda_1 + S_1 S_2}{\Lambda_1 \Lambda_2 (1-S^2)} \right] = B_{f2} + A_2 H. \quad (37b)$$

Here, the first terms are the magnetic induction of the fluxon,  $B_f$ , and the second terms represent uniform magnetic-field penetration into the JJ with thin electrodes.

Substituting Eq. (37) into Eqs. (27), (28), and (32) we obtain the equation for the Gibbs free-energy density

$$\mathbf{G}(B) = \mathbf{G}_J - \frac{H}{4\pi} [B_{f1} \Lambda_1^* + B_{f2} \Lambda_2^*], \quad (38)$$

where

$$\mathbf{G}_J = \sum J_{ci} [1 - \cos(\varphi_i)] + \frac{1}{8\pi} [B_{f1}^2 \Lambda_1 - 2B_{f1} B_{f2} S_2 + B_{f2}^2 \Lambda_2], \quad (39)$$

is the Josephson energy. In Eq. (38) we skipped terms  $\sim H^2$  which are not important for minimizing  $\mathbf{G}(B)$ .

From Eqs. (38) and (39) it is seen that  $\mathbf{G}(B)$  is a bilinear form of  $B_{f1,2}$  which can be minimized in different ways for different relations between  $B_{f1}$  and  $B_{f2}$ , Eq. (37). In other words,  $\mathbf{G}(B)$  has a particular minimum for each particular fluxon mode  $(n_1, n_2)$ .

The lower critical field corresponds to the state with a fluxon in the weakest junction (JJ1) and no fluxons in the second JJ. Thus to obtain  $H_{c1}$  we should minimize  $\mathbf{G}(B)$  with respect to the number of fluxons in JJ1 for the fluxon mode  $(n, 0)$ . After integration of Eq. (38) along the  $x$  axis we finally obtain

$$H_{c1} = \frac{4\pi E(1,0)}{\Phi^*}, \quad (40)$$

where

$$\Phi^* = \Phi_0 \left( \frac{\Lambda_1^* \Lambda_2 + \Lambda_2^* S_2}{\Lambda_1 \Lambda_2 (1-S^2)} \right), \quad (41)$$

and  $E(1,0)$  is the free energy of a single fluxon in JJ1 obtained in the previous section. Note that  $\Phi^*$  in Eq. (41) is equal to the flux carried by a fluxon. For junctions with identical superconducting electrodes,  $d \ll \lambda_s$ ,

$$H_{c1} \cong \frac{4\pi E(1,0)}{\Phi_0} \frac{\lambda_s^2}{d(t+d)}, \quad (42)$$

which in this limit has the same structure as that for a single junction, Eq. (36), but with larger total fluxon energy as shown in Fig. 4.

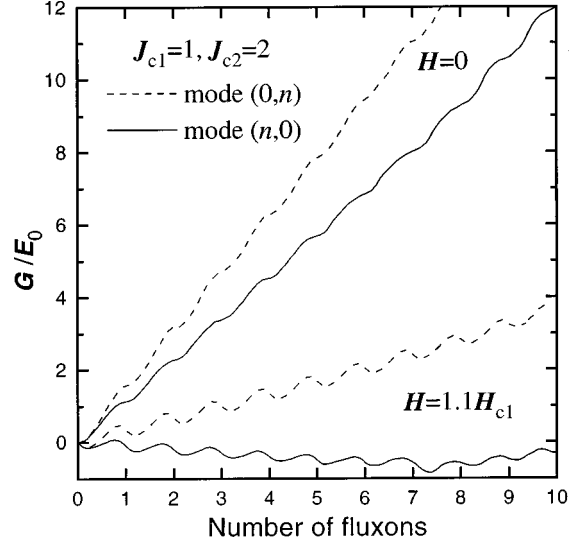


FIG. 5. Gibbs free energy versus the number of fluxons for  $H=0$ , and  $H$  slightly larger than  $H_{c1}$  for two particular fluxon modes,  $(n,0)$  and  $(0,n)$  corresponding to fluxons in JJ1 and JJ2, respectively. Parameters of the stack are  $J_{c1}=1$ ,  $J_{c2}=2$ ,  $\lambda_{s1}=\lambda_{s2}=\lambda_{s3}=0.1\lambda_{J1}$ ,  $t_1=t_2=d_1=d_2=d_3=0.01\lambda_{J1}$ ,  $L_x=50\lambda_{J1}$ , and  $S \approx 0.5$ .

Figure 5 shows  $\mathbf{G}(B)$  versus the number of fluxons for  $H=0$ , and  $H$  slightly larger  $H_{c1}$  for two particular fluxon modes,  $(n,0)$  and  $(0,n)$ . Solid lines represent mode  $(n,0)$  and show  $\mathbf{G}(B)$  as a function of fluxons in JJ1 with no fluxons in JJ2. Dashed lines represent mode  $(0,n)$  and show  $\mathbf{G}(B)$  as a function of fluxons in JJ2 with no fluxons in JJ1. The number of fluxons in the JJ's is measured by the total phase shift along the junction length divided by  $2\pi$ . Parameters of the stack are  $J_{c1}=1$ ,  $J_{c2}=2$ ,  $\lambda_{s1}=\lambda_{s2}=\lambda_{s3}=0.1\lambda_{J1}$ ,  $t_1=t_2=d_1=d_2=d_3=0.01\lambda_{J1}$ ,  $L_x=50\lambda_{J1}$ , and  $S \approx 0.5$ . In Fig. 6, a contour plot of Gibbs free energy versus

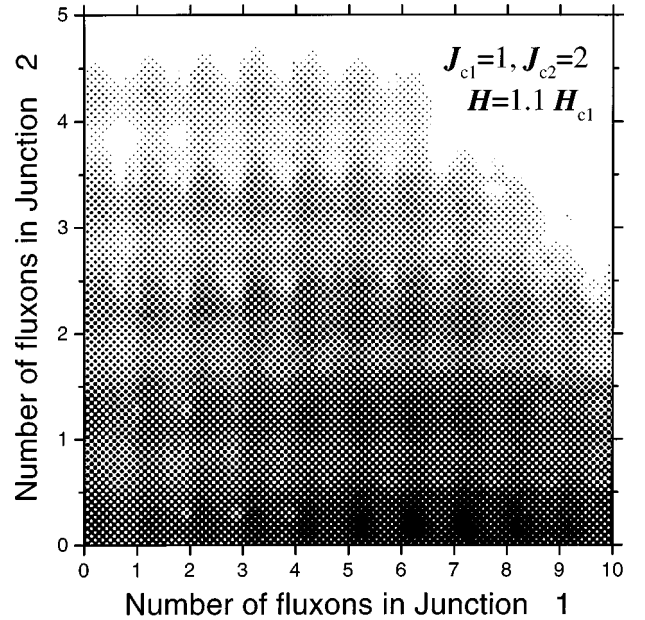


FIG. 6. Gray scale plot of Gibbs free energy versus the number of fluxons in junctions 1 and 2 for  $H=1.1H_{c1}$ . Parameters of the stack are the same as in Fig. 5. Darker regions correspond to smaller Gibbs energy. The existence of various quasiequilibrium states can be seen.

the number of fluxons in junctions 1 and 2 is shown in gray scale for  $H \approx 1.1H_{c1}$ . Parameters of the stack are the same as in Fig. 5. Darker regions correspond to smaller Gibbs energy, the absolute minimum of Gibbs free energy is achieved around  $n_1 = 7$  and  $n_2 \sim 0$ .

Figure 5 shows that at zero magnetic field the minimum of  $\mathbf{G}(B)$  corresponds to the Meissner state with  $n_1 = n_2 = 0$ . For  $H > H_{c1}$  the absolute minimum is achieved for a particular fluxon mode  $(n_1, n_2)$ , e.g., for the case of Figs. 5, 6 the absolute minimum is achieved for the  $(7, 0)$  mode. This mode corresponds to thermodynamically equilibrium state. However, from Figs. 5, 6 it is seen that besides the absolute minimum there are a number of other fluxon modes for which the local minimum of the Gibbs free energy is achieved. All those modes are stable and represent the possible quasiequilibrium states in the stack.

### III. FLUXON DYNAMICS

The dynamic behavior of SJJ's is characterized first of all by the existence of several limiting Swihart velocities. In the case of a double stack there are two characteristic Swihart velocities  $\tilde{c}_{1,2}$ , see Eq. (21). Thus, the behavior of the stack should be different for  $u < \tilde{c}_1$  and  $\tilde{c}_1 < u < \tilde{c}_2$ . Here we restrict ourselves to consider the single soliton state, mode  $(1,0)$ . Note that this state is neither the in-phase nor the out-of-phase state discussed in the literature<sup>18,4,24</sup> because we always have a zero total phase shift in JJ2.

For  $u < \tilde{c}_1$  a pure traveling soliton solution exists and is given by Eq. (25). When  $u \rightarrow \tilde{c}_1$  a Lorentz contraction of the soliton takes place since  $\gamma_1 \rightarrow 0$ , see Eq. (19).

For  $\tilde{c}_1 < u < \tilde{c}_2$ ,  $\gamma_1$  becomes purely imaginary. This means that the  $F_1$  component in Eq. (25) transforms to a traveling plasma wave

$$F_1 = \exp(ik_1(x - ut)), \quad (43)$$

where

$$k_1^{-2} = \lambda_1^2 \left( \frac{u^2}{\tilde{c}_1^2} - 1 \right).$$

The only possible pure traveling soliton solution in this case is given by a single component special solution  $F_2$ , Eq. (18b). Such soliton will survive until  $u \leq \tilde{c}_2$ . For higher velocities, the  $F_2$  component will also turn to a traveling plasma wave.

In Fig. 7, the instantaneous spatial profiles of the voltages  $V_{1,2}$

$$V_{1,2} = \frac{\Phi_0}{2\pi c} \dot{\phi}_{1,2},$$

in junctions 1 and 2 are shown by solid and dashed lines, respectively, for four different fluxon velocities,  $u = 0.5 < \tilde{c}_1$ ,  $u = 0.81 \approx \tilde{c}_1$ ,  $\tilde{c}_1 < u = 1 < \tilde{c}_2$ ,  $u = 1.37 \approx \tilde{c}_2$ , see Table I. The profiles were obtained from the analytic solution for a single fluxon in JJ1, mode  $(1,0)$  in a double stack with identical junctions  $\lambda_{s1} = \lambda_{s2} = \lambda_{s3} = 0.1\lambda_{J1}$ ,  $t_1 = t_2 = d_1 = d_2 = d_3 = 0.01\lambda_{J1}$ , and  $S \approx 0.5$ . The voltage is normalized to  $V_0 = \Phi_0 \omega_{p1} / 2\pi c$ . The plots for different velocities were shifted with respect to each other for clarity. From Fig. 7 it is seen that the voltage in the second junction at the fluxon origin,

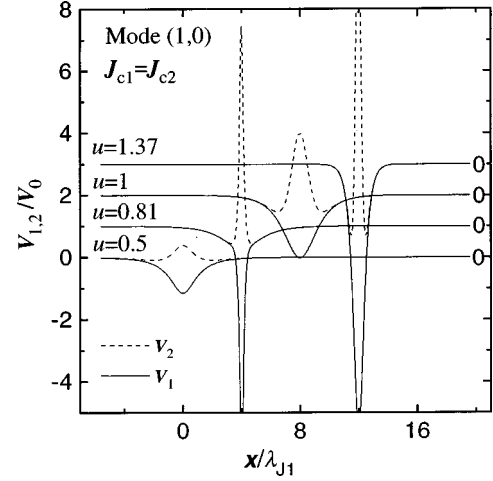


FIG. 7. Instantaneous spatial profiles of the voltages  $V_{1,2}$  in junctions 1 (solid lines) and 2 (dashed lines) generated by the motion of a single fluxon in JJ1, mode  $(1,0)$  for four different fluxon velocities,  $u = 0.5 < \tilde{c}_1$ ,  $u = 0.81 \approx \tilde{c}_1$ ,  $\tilde{c}_1 < u = 1 < \tilde{c}_2$ ,  $u = 1.37 \approx \tilde{c}_2$ . The profiles were obtained for a double stack with identical junctions with  $\lambda_{s1} = \lambda_{s2} = \lambda_{s3} = 0.1\lambda_{J1}$ ,  $t_1 = t_2 = d_1 = d_2 = d_3 = 0.01\lambda_{J1}$ ,  $S \approx 0.5$ . The plots for different velocities were shifted with respect to each other for clarity.

$V_2(0)$ , always has an opposite sign with respect to  $V_1(0)$ . Note that  $V_1$  has nonzero average value, while the average value of  $V_2$  is equal to zero since there is no total phase shift in JJ2.

#### A. Attractive fluxon interaction

In Fig. 8, the instantaneous spatial profiles of the magnetic induction  $B_{1,2}$ , Eq. (37), in junctions 1 and 2 are shown by the solid and dashed lines, respectively, for five different fluxon velocities, which are the static case  $u = 0$ , and the

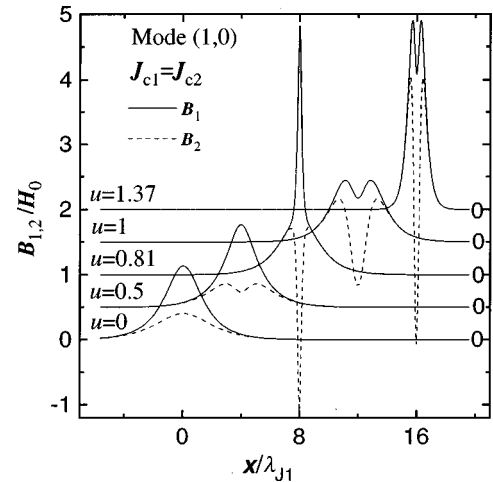


FIG. 8. Instantaneous spatial profiles of the magnetic induction  $B_{1,2}$  in junctions 1 (solid lines) and 2 (dashed lines) for a single fluxon in JJ1, mode  $(1,0)$  and for different fluxon velocities,  $u = 0$ ,  $u = 0.5 < \tilde{c}_1$ ,  $u = 0.81 \approx \tilde{c}_1$ ,  $\tilde{c}_1 < u = 1 < \tilde{c}_2$ ,  $u = 1.37 \approx \tilde{c}_2$ . The profiles were obtained for a double stack with identical JJ's, similar to that in Fig. 7. The plots for different velocities were shifted with respect to each other for clarity. It is seen that at high velocities  $B_2(0)$  changes the sign resulting in attractive fluxon interaction in adjacent JJ's.

dynamic ones  $u = 0.5 < \tilde{c}_1$ ,  $u = 0.81 \approx \tilde{c}_1$ ,  $\tilde{c}_1 < u = 1 < \tilde{c}_2$ ,  $u = 1.37 \approx \tilde{c}_2$ . The profiles were obtained from the analytic solution for a single fluxon in JJ1, mode (1,0) in a double stack with the same parameters as in Fig. 7. The magnetic field is normalized to  $H_0 = \Phi_0 / (\pi \Lambda_1 \lambda_{J1})$ . The plots for different velocities were shifted with respect to each other for clarity. From Fig. 8 it is seen that at low velocities the magnetic induction in the second junction  $B_2$  has the same sign as  $B_1$ , see also Fig. 2(b). With increasing velocity a dip in  $B_2(0)$  at the fluxon origin appears which is developed with increasing fluxon velocity and at high velocities changes the sign with respect to  $B_1(0)$ . We emphasize that unlike the single JJ the magnetic induction  $B_i$  in the stack is not given by the spatial derivative of the phase  $\varphi'_i$  as it some times can be seen in literature,<sup>24</sup> but rather is defined in a more complicated way, see Eqs. (37,1).

The origin of the sign change of  $B_2(0)$  can be most clearly seen for the case  $\tilde{c}_1 < u < \tilde{c}_2$ . In this case the soliton solution corresponds to the single-component special solution  $F_2$ , Eq. (18b). At the fluxon origin,  $\varphi'_1$  and  $\varphi'_2$  have different signs, while the weight coefficient for  $\varphi'_2$  is larger than that for  $\varphi'_1$ ,  $\Lambda_1 > S_2$ , see Eq. (37b).

Now if we suppose that there is a fluxon in JJ2, it would tend to be attracted to the region with  $B_2 < 0$ . Then the so-called *in-phase* state with fluxons one on the top of the other in the adjacent JJ's may become favorable in the dynamic state with high enough fluxon velocity. A possible indication of such unusual phase-locked state has been observed recently by low-temperature scanning electron microscopy (LTSEM).<sup>25</sup>

### B. Fluxon modes and $I$ - $V$ curve

From the analysis made above, we can make conclusions about the overall  $I$ - $V$  curve of a double stack in an experimental situation. For a given fluxon mode we can distinguish three branches in the  $I$ - $V$  curve. (i)  $u < \tilde{c}_1$ . This is the lower flux-flow branch for which the soliton solution is given by Eq. (25). (ii)  $\tilde{c}_1 < u < \tilde{c}_2$ . This is the upper flux-flow branch. Here, the only possible soliton solution is given by the special solution in Eq. (18b). Simultaneously we would expect a strong plasma wave generation in both JJ's of the form of Eq. (43) so that the general propagating wave is given by the superposition of a soliton  $F_2$ , Eq. (18b) and plasma waves from a degenerated  $F_1$  component, Eq. (43). (iii)  $u > \tilde{c}_2$ . At this branch only plasma waves exist with two different dispersion laws

$$\omega_{1,2}^2 = \tilde{c}_{1,2}^2 (k_{1,2}^2 + \lambda_{1,2}^{-2}). \quad (44)$$

As we mentioned in Sec. II B, for the  $N$ -fold stack there are  $N$  characteristic Swihart velocities providing  $N$  distinct flux-flow branches in the  $I$ - $V$  curve for a particular fluxon mode. However, the possible number of branches in the  $I$ - $V$  curve is not limited by the number of JJ's in the stack. As it is shown in Sec. II D, there are various quasiequilibrium fluxon modes in a given external magnetic field. In addition, a given number of fluxons can be arranged in the stack in different manners, each corresponding to a particular fluxon mode. Different fluxon modes will in general have different characteristic Swihart velocities. For example, let us consider

the (1,0) and (0,1) modes in a stack of two JJ's corresponding to a single fluxon in JJ1 and JJ2, respectively. It is clear that mode (0,1) is given by a solution for mode (1,0) with the inverted ratio  $J_{c2}/J_{c1}$ . For example, mode (0,1) in the stack with  $J_{c2}/J_{c1} = 0.1$  is identical to mode (1,0) in the stack with  $J_{c2}/J_{c1} = 10$ . From Table I we see that modes (1,0) and (0,1) have different characteristic velocities. The only case when modes (1,0) and (0,1) are identical is the case of double stack with identical JJ's. Already for a threefold stack with identical JJ's modes (1,0,0) and (0,1,0) have different Swihart velocities and modes (1,0,0) and (0,0,1) are identical.

In general for a stack with  $N$  nonidentical JJ's with, in total,  $M$  fluxons, the total possible number of different fluxon modes is equal to

$$m = \frac{(N+M-1)!}{(N-1)!M!}, \quad (45)$$

each having  $N$  different characteristic Swihart velocities. Thus the total number of possible  $I$ - $V$  branches is

$$n = mN, \quad (46)$$

which can be much larger than  $N$ .

## IV. DISCUSSION

As we have shown above, the obtained analytical fluxon solution in Eq. (25) provide not only qualitative but also a fairly good quantitative approximation for  $\varphi_1$  since it satisfies asymptotically Eq. (12) for  $x \ll -1$ ,  $x \sim 0$  and  $x \gg 1$ . Previously, a linearized version of the coupled sine-Gordon equation have been considered,<sup>19</sup> however, the solution was obtained only for traveling waves, Eq. (43), which certainly is very different from the propagating soliton solution obtained here. We admit that the traveling-wave approach can provide the correct values for the characteristic penetration depths, Eq. (20), and Swihart velocities, Eq. (21), of the SJJ. However, in previous analysis<sup>18,19,22-24</sup> it was not realized that the fluxon solution in SJJ's cannot be described by a single penetration depth. This can be clearly seen from Fig. 2(a) which illustrates that the decay lengths of currents in junctions 1 and 2 are different. This is a general property of a system of coupled equations with different characteristic lengths. For the case of  $N$  JJ's in the stack, the solution for a particular single fluxon mode (0,...0,1,0,...0) is described in a unique way by  $N$  different characteristic lengths, similar to Eq. (25). Note that for  $N > 2$ , even for SJJ's with identical parameters, different fluxon modes are in general described by different sets of  $N$  characteristic lengths and velocities.

From Figs. 5 and 6 it is seen that there are a lot of local minimums of the Gibbs free energy corresponding to different fluxon modes, each representing a quasiequilibrium state of the SJJ. Under these circumstances we expect a pronounced hysteretic behavior and a prehistory dependence in SJJ's associated with transitions between quasiequilibrium fluxon modes. As was discussed in Ref. 8, this might be the reason for having complicated and not well-defined Fraunhofer patterns in "long" SJJ's with  $L_x > \lambda_J$ . This is in qualitative agreement with Fraunhofer patterns observed for Nb/AIO<sub>x</sub>/Nb,<sup>5</sup> Nb/Cu multilayers<sup>8</sup> and HTSC's.<sup>1,10,11</sup>

As we mentioned in Sec. II C, there is a certain discrepancy in the literature about the estimation of the fluxon free energy and the lower critical field.<sup>22,23</sup> From the numerical

simulations and the analysis based on the approximate analytic solution we claim that the fluxon energy in the stack is always larger than that of a single JJ, see Fig. 4. More serious disagreement exists in estimations of  $H_{c1}$ . In the limit of thin layers,  $d \ll \lambda_s$ ,  $H_{c1}$  of Ref. 22 is about  $(\lambda_s/d)^2 \gg 1$  times smaller than our result given by Eq. (42). Such discrepancy is caused by disregarding the  $E_H$  term, Eq. (30), in the Hamiltonian of Ref. 22 and consequently disregarding the free magnetic-field penetration in thin layered SJJ's. With increasing number of layers the total flux of the fluxon increases and approaches  $\Phi_0$ . For the infinite stack with thin layers the lower critical field was derived in Refs. 14–16 for identical JJ's and in Ref. 17 for nonidentical JJ's  $H_{c1}$  in this case is in the range predicted by Eq. (33).

From the analysis of the dynamic behavior of SJJ's we show that the attractive interaction of fluxons in adjacent junctions appears at high enough fluxon velocity. This will lead to the possibility of having an in-phase fluxon mode with fluxons on top of each other. Recently, a possible indication of such state has been observed by LTSEM.<sup>25</sup>

We note however that it is not necessary to have two different in-phase and out-of-phase fluxon modes to observe two distinct flux-flow branches in the  $I$ - $V$  curve of a double SJJ. As we show,  $N$  flux-flow branches exist for each particular fluxon mode which is simply a consequence of existence of  $N$  different Swihart velocities. An important consequence of this is a possibility of having  $n > N$  flux-flow branches in the  $I$ - $V$  curve of the SJJ, see Eq. (46). Such behavior was observed for Nb/Cu multilayers in parallel magnetic field.<sup>8</sup> Of course not all of the  $n$   $I$ - $V$  curve branches should be observable in experiment. Analysis with

respect to stability of different modes in the dynamic state should be performed.

## V. CONCLUSIONS

In conclusion static and dynamic properties of nonidentical stacked Josephson junctions were studied theoretically. An approximate analytic solution for a stack with arbitrary parameters was obtained. Characteristic penetration depths, Swihart velocities, the lower critical field, the first integral, and the free energy for a stack of nonidentical junctions were derived and studied for different parameters of the stack. We show that attractive interaction of fluxons in adjacent junctions exists in the dynamic state of the stack leading to appearance of the in-phase state in SJJ's. In a given external magnetic field the Gibbs free energy has a number of local minima corresponding to particular fluxon modes in the stack, each representing a quasiequilibrium state. For a stack of  $N$  junctions, each mode would result in  $N$  distinct flux-flow branches in the  $I$ - $V$  curve. Taking into account that different modes with equal total number of fluxons are not identical we conclude that the total possible number of flux-flow branches can be much larger than the number of junctions in the stack.

## ACKNOWLEDGMENTS

We are indebted to A. Yurgens and N. Mros for stimulating discussions. The work was supported by the Swedish Superconductivity Consortium and in part by the Russian Foundation for Basic Research under Grant No. 96-02-19319.

- 
- <sup>1</sup>R. Kleiner, F. Steinmeyer, G. Kunkel, and P. Mueller, Phys. Rev. Lett. **68**, 2394 (1992); R. Kleiner and P. Mueller, Phys. Rev. B **49**, 1327 (1994).
- <sup>2</sup>A. Yurgens, D. Winkler, N. V. Zavaritsky, and T. Claeson, Phys. Rev. B **53**, R8887 (1996).
- <sup>3</sup>M. G. Blamire, E. C. G. Kirk, J. E. Evetts, and T. M. Klapwijk, Phys. Rev. Lett. **66**, 220 (1991).
- <sup>4</sup>A. V. Ustinov, M. Cirillo, H. Kohlstedt, G. Hallmanns, C. Heiden, and N. F. Pedersen, Phys. Rev. B **48**, 10 614 (1993).
- <sup>5</sup>H. Amin, M. G. Blamire, and J. E. Evetts, IEEE Trans. Appl. Supercond. **3**, 2204 (1993); H. Kohlstedt, G. Hallmanns, I. P. Nevirkovets, D. Guggi, and C. Heiden, *ibid.* **3**, 2197 (1993).
- <sup>6</sup>V. M. Krasnov, A. E. Kovalev, V. A. Oboznov, and V. V. Ryzanov, Physica C **215**, 265 (1993).
- <sup>7</sup>V. M. Krasnov, N. F. Pedersen, V. A. Oboznov, and V. V. Ryzanov, Phys. Rev. B **49**, 12 969 (1994).
- <sup>8</sup>V. M. Krasnov, A. E. Kovalev, V. A. Oboznov, and N. F. Pedersen, Phys. Rev. B **54**, 15 448 (1996).
- <sup>9</sup>S. Wahlsten, S. Runder, and T. Claeson, J. Appl. Phys. **49**, 4248 (1978).
- <sup>10</sup>D. C. Ling, G. Yong, J. T. Chen, and L. E. Wenger, Phys. Rev. Lett. **75**, 2011 (1995).
- <sup>11</sup>Yu. I. Latyshev and J. E. Nevelskaya, Physica C **235–240**, 2991 (1994).
- <sup>12</sup>J. U. Lee, J. E. Nordman, and G. Hohenwarter, Appl. Phys. Lett. **67**, 1471 (1995).
- <sup>13</sup>Y. Matsuda, M. B. Gaifullin, K. Kumagai, K. Kadowaki, and T. Mochiku, Phys. Rev. Lett. **75**, 4512 (1995).
- <sup>14</sup>W. E. Lawrence and S. Doniach, in *Proceedings of the 12th International Conference on Low Temperature Physics, Kyoto 1970*, edited by E. Kanda (Academic press of Japan, Kyoto, 1971), p. 361.
- <sup>15</sup>L. N. Bulaevskii, Sov. Phys. JETP **64**, 2241 (1973).
- <sup>16</sup>J. R. Clem and M. W. Coffey, Phys. Rev. B **42**, 6209 (1990).
- <sup>17</sup>A. A. Golubov and V. M. Krasnov, Physica C **196**, 177 (1992); V. M. Krasnov, N. F. Pedersen, and A. A. Golubov, Physica C **209**, 579 (1993).
- <sup>18</sup>S. Sakai, P. Bodin, and N. F. Pedersen, J. Appl. Phys. **73**, 2411 (1993).
- <sup>19</sup>S. Sakai, A. V. Ustinov, H. Kohlstedt, A. Petraglia, and N. F. Pedersen, Phys. Rev. B **50**, 12 905 (1994).
- <sup>20</sup>M. Tachiki, T. Koyama, and S. Takahashi, Phys. Rev. B **50**, 7065 (1994); L. N. Bulaevskii, M. P. Maley, and M. Tachiki, Phys. Rev. Lett. **74**, 801 (1995).
- <sup>21</sup>T. Koyama and M. Tachiki, Phys. Rev. B **54**, 16 183 (1996).
- <sup>22</sup>S. N. Song, P. R. Auvil, M. Ulmer, and J. B. Ketterson, Phys. Rev. B **53**, R6018 (1996).
- <sup>23</sup>E. Goldobin, A. Golubov, and A. V. Ustinov, Czech. J. Phys. **46** Suppl. S2, 663 (1996).
- <sup>24</sup>A. Pertaglia, A. V. Ustinov, N. F. Pedersen, and S. Sakai, J. Appl. Phys. **77**, 1171 (1995).
- <sup>25</sup>I. P. Nevirkovets, T. Doderer, A. Laub, M. G. Blamire, and J. E. Evetts, J. Appl. Phys. **80**, 2321 (1996).